



# Evaluation and categorisation of individual patients based on white matter profiles: Single-patient diffusion data interpretation in neurodegeneration

Marlene Tahedl<sup>a,b</sup>, Aizuri Murad<sup>a</sup>, Jasmin Lope<sup>a</sup>, Orla Hardiman<sup>a</sup>, Peter Bede<sup>a,c,\*</sup>

<sup>a</sup> Computational Neuroimaging Group, Trinity College Dublin, Dublin, Ireland

<sup>b</sup> Department of Psychiatry and Psychotherapy, Institute for Psychology, University of Regensburg, Germany

<sup>c</sup> Pitié-Salpêtrière University Hospital, Sorbonne University, Paris, France

## ARTICLE INFO

### Keywords:

Amyotrophic lateral sclerosis  
Neuroimaging  
MRI  
Diagnostic classification  
Biomarker  
Precision medicine

## ABSTRACT

The majority of radiology studies in neurodegenerative conditions infer group-level imaging traits from group comparisons. While this strategy is helpful to define phenotype-specific imaging signatures for academic use, the meaningful interpretation of single scans of individual subjects is more important in everyday clinical practice. Accordingly, we present a computational method to evaluate individual subject diffusion tensor data to highlight white matter integrity alterations. Fifty white matter tracts were quantitatively evaluated in 132 patients with amyotrophic lateral sclerosis (ALS) with respect to normative values from 100 healthy subjects. Fractional anisotropy and radial diffusivity alterations were assessed individually in each patient. The approach was validated against standard tract-based spatial statistics and further scrutinised by the assessment of 78 additional data sets with a blinded diagnosis. Our z-score-based approach readily detected white matter degeneration in individual ALS patients and helped to categorise single subjects with a 'blinded diagnosis' as likely 'ALS' or 'control'. The group-level inferences from the z-score-based approach were analogous to the standard TBSS output maps. The benefit of the z-score-based strategy is that it enables the interpretation of single DTI datasets as well as the comparison of study groups. Outputs can be summarised either visually by highlighting the affected tracts, or, listing the affected tracts in a text file with reference to normative data, making it particularly useful for clinical applications. While individual diffusion data cannot be visually appraised, our approach provides a viable framework for single-subject imaging data interpretation.

## 1. Introduction

White matter alterations are an early feature of amyotrophic lateral sclerosis (ALS) and can already be discerned in the presymptomatic phase of the disease. [1–6] The core white matter signature of ALS includes corpus callosum and corticospinal tract degeneration [7] often with varying degree of frontotemporal and cerebellar white matter pathology. [8,9] Frontotemporal white matter changes have been described in the uncinate fasciculus, cingulum, fornix, superior longitudinal fasciculus, anterior thalamic radiation, forceps minor, inferior longitudinal fasciculus. [10–12] Widespread extra-motor white matter degeneration has been initially linked to C9orf72 hexanucleotide repeat expansions, [13] but more recent studies confirmed that frontotemporal disease burden is not unique to this genotype. [14] The majority of white matter studies in ALS report group-level findings based on comparative

models which are useful for the characterisation of specific phenotypes and genotypes. Some white matter studies adopt a correlation strategy, to explore the anatomical underpinnings of specific clinical symptoms, but often, a considerable dissociation exists between clinical and radiological observations. [15] Longitudinal imaging studies suggest that white matter changes in ALS may be readily detected around the time of the diagnosis, often earlier than cortical grey matter atrophy, but white matter changes exhibit relatively limited further progression on follow-up imaging. [16,17] The observation that disease-specific white matter signatures are an early and relatively consistent feature of ALS supports the role of white matter imaging in diagnostic classification algorithms. White matter parameters have been used in a multitude of categorisation frameworks including support-vector machines, discriminant function analyses, logistic regression, and random forest models with varying diagnostic classification accuracy. [18–23] The pitfalls of building models on smaller training datasets are well

\* Corresponding author: Computational Neuroimaging Group, Trinity College Dublin, Room 5.43, Trinity Biomedical Sciences Institute, 152-160 Pearse Street, Dublin 2, Ireland.

E-mail address: [bedep@tcd.ie](mailto:bedep@tcd.ie) (P. Bede).

<https://doi.org/10.1016/j.jns.2021.117584>

Received 3 July 2021; Received in revised form 13 July 2021; Accepted 19 July 2021

Available online 21 July 2021

0022-510X/© 2021 The Authors.

Published by Elsevier B.V. This is an open access article under the CC BY-NC-ND license

(<http://creativecommons.org/licenses/by-nc-nd/4.0/>).

**Glossary**

AD	axial diffusivity	MDT	Multi-disciplinary team
AF	arcuate fasciculus	MND	Motor neuron disease
ALS	amyotrophic lateral sclerosis	MNI152	Montreal Neurological Institute 152 standard space
ALSFRS-r	revised amyotrophic lateral sclerosis functional rating scale	MP-PCA	Marcenko-Pastur principal component analysis
ANCOVA	analysis of covariance	MRC	Medical Research Council Scale for Muscle Strength
C9orf72	chromosome 9 open reading frame 72	NODDI	neurite orientation dispersion and density imaging
CSD	Constrained Spherical Deconvolution	PBA	Pseudobulbar affect
DFA	discriminant function analysis	PCC	Pathological crying and laughing
DKI	diffusion kurtosis imaging	PLS	primary lateral sclerosis
DTI	Diffusion Tensor Imaging	PMA	Progressive muscular atrophy
DW	diffusion-weighted data	PUMNS	Penn Upper Motor Neuron Score
EMM	estimated marginal mean	RD	radial diffusivity
FA	fractional anisotropy	QSM	quantitative susceptibility mapping
FLAIR	Fluid-attenuated inversion recovery	ROI	region of interest
FOV	field of view	Rt	Right
FTD	Frontotemporal dementia	SBMA	Spinal and bulbar muscular atrophy / Kennedy's disease
FTLD	frontotemporal lobar degeneration	SD	standard deviation
FWE	familywise error	SE-EPI	spin-echo echo planar imaging
GM	grey matter	SENSE	Sensitivity Encoding
HADS	hospital anxiety and depression scale	SLF	superior longitudinal fasciculus
HARDI	high angular resolution diffusion imaging	SMA	Spinal muscular atrophy
HC	healthy control	SPIR	spectral presaturation with inversion recovery
HSP	hereditary spastic paraplegia	SVM	support vector machine
IR-SPGR	inversion recovery prepared spoiled gradient recalled echo	T1W	T1-weighted imaging
IR-TSE	inversion recovery turbo spin echo sequence	TE	Echo time
LMN	lower motor neuron	TFCE	threshold-free cluster enhancement
Lt	Left	TI	Inversion time
MD	mean diffusivity	TIV	total intracranial volume
		TR	repetition time
		UMN	Upper motor neuron

recognised, chief of which is the overfitting of such models to the training data which results in poor generalisability. [24] While the description of group-level white matter signatures and stereotyped propagation patterns is academically relevant, the pragmatic demands of clinical imaging are markedly different. In clinical practice, the characterisation of shared imaging traits among many patients is a lower priority compared to the precision interpretation of MR data from single subjects. The evaluation of imaging data in single subjects is hugely important across a variety of clinical scenarios such as the assessment of 'suspected' patients exhibiting limited clinical findings, the appraisal of datasets from family members fearing a potential diagnosis, the follow-up of confirmed cases to appraise progressive changes etc. In line with the practical objectives of clinical imaging, the objective of our study is the development, testing and validation of a quantitative imaging framework to interpret individual diffusion datasets.

## 2. Methods

### 2.1. Participants

The study has two arms; (1) a descriptive part, where white matter (WM) changes are evaluated in subjects with a known diagnosis and (2) a pilot, proof-of concept arm where the diagnosis of the participants are blinded. In the descriptive arm of the study 132 patients with amyotrophic laterals sclerosis (ALS) and 100 healthy controls (HC) were included. In the pilot classification part of the study, 53 patients with ALS and 25 HC were included. A total of 185 patients and 125 controls were included. Patients were diagnosed according to the El Escorial criteria and patients with prior traumatic brain injury, comorbid neurovascular, neuroinflammatory or neoplastic conditions were excluded. The healthy controls included in this study were not related to

participating patients, and had no known family history of neurodegenerative disorders. All participants provided informed consent in accordance with the ethics approval of the project. (Ethics Medical Research Committee - Beaumont Hospital, Dublin, Ireland).

### 2.2. Magnetic resonance imaging

Diffusion tensor imaging (DTI) data were acquired on a 3 Tesla Philips Achieva Magnetic resonance (MR) platform using a spin-echo echo planar imaging (SE-EPI) pulse sequence with a 32-direction Stejskal-Tanner diffusion encoding scheme, FOV =  $245 \times 245 \times 150$  mm, 60 slices with no interslice gaps, spatial resolution =  $2.5 \text{ mm}^3$ , TR/TE = 7639 / 59 ms, b-values = 0, 1100 s/mm<sup>2</sup>, SENSE factor = 2.5, acquisition time: 5 min 41 s, dynamic stabilisation and spectral pre-saturation with inversion recovery (SPIR) fat suppression. For clinical interpretation, FLAIR images of each participant were also reviewed. FLAIR imaging took place in axial orientation using an Inversion Recovery Turbo Spin Echo (IR-TSE) sequence: TR/TE = 11,000 / 125 ms, TI = 2800 ms, FOV =  $230 \times 183 \times 150$  mm, spatial resolution =  $0.65 \times 0.87 \times 4$  mm, 120° refocusing pulse, with flow compensation and motion smoothing and a saturation slab covering the neck region. A 3D Inversion Recovery prepared Spoiled Gradient Recalled echo (IR-SPGR) sequence was implemented to record T1-weighted (T1w) images with the following settings: field-of-view (FOV) of  $256 \times 256 \times 160$  mm, flip angle = 8°, spatial resolution of  $1 \text{ mm}^3$ , SENSE factor = 1.5, acquisition time: 7 min 30 s, TR/TE = 8.5/3.9 ms, TI = 1060 ms.

### 2.3. Diffusion-weighted (DW) data processing

Pre-processing of DW data was performed within *MRtrix3* [25] and noise corrections using the Marcenko-Pastur principal component

analysis (MP-PCA), [26,27] removal of Gibb's Ringing Artifacts [28], correction for motion and eddy currents [29] and bias field correction using the N4 method as implemented in the ANTs software. [30] DW data were then co-registered to align with the T1-weighted data using a linear registration scheme with six degrees of freedom, where the  $b = 0$  image served as a source and the raw T1-weighted image as the target data. Subsequently, the diffusion tensor model was fitted to the pre-processed DW-images [31] and for each subject, fractional anisotropy (FA) and radial diffusivity (RD) maps were extracted. T1-weighted images were skull-stripped and biasfield-corrected within FSL. [32,33] Version 6.0 of FMRIB'S FSL was used. The peaks of the spherical harmonic function in each voxel were extracted by first estimating the response function for spherical deconvolution in each subject separately using the *dhollander* algorithm [34] and then estimating fibre orientation distributions following a multi-shell approach. Since two shells were acquired,  $b = 1000$  and  $b = 0$ , the response functions for both WM and CSF could be estimated. The results were normalised using a multi-tissue informed log-domain intensity normalisation scheme [35] and the peaks of the spherical harmonic function from that normalised image. [36]

#### 2.4. z-score based interpretation of individual datasets

To test each individual subject WM microstructure alterations with respect to healthy controls, bundle-specific tractograms were first generated for each subject based on the estimated peaks of the spherical harmonic function. [37] DW data were segmented using *TractSeg* into 50 anatomically labelled tracts and FA / RD were estimated along 100 points of each tract. These estimates were averaged along each tract to generate a single proxy of WM microstructure integrity per subject and tract. Data from HCs were used as normative data, building distributions of the averaged and z-scored WM metrics separately for male and female patients. Normative data were used to test whether individual subjects' WM profile differed from the sex-matched 'physiological' range. Each patient's tractwise z-scores were calculated with reference to their demographically-appropriate control group and then z-scores were converted to p-values. Two statistical tests were run to identify tracts

with FA reductions and tracts with increased RD using an alpha-level threshold of  $p < 0.025$  below which we considered an individual patient's tract as 'affected'. In addition to individual subject WM rating, group level contrasts have also been performed using Monte-Carlo permutation to estimate family-wise error-corrected p-values for each tract. First, nonparametric null distributions were created for each tract to estimate the expected frequencies of patients for which 'significant' changes were observed as a random process. Random scalars were drawn from a binomial distribution, where the total number of patients was used as parameter  $n$  (reflecting the number of trials) and the selected alpha-threshold of 0.025 as parameter  $p$  (reflecting the probability of occurrence). This process was repeated 100,000 times for each tract. The parameter  $n$  was different for each tract since tract segmentation using *TractSeg* failed in some patients for a subset of tracts (Table 1). The number of patients exhibiting WM alterations in each tract was determined providing the vector of size  $n_{\text{tracts}}$ . These observed frequencies were then converted into p-values by establishing how many of the randomly generated frequencies exceeded the observed count and dividing by that count by the number of iterations (100,000). The significance level was set to  $p < 0.01$ .

#### 2.5. Cross-validation by the standard approach

For validation purposes, standard tract-based spatial statistics (TBSS) were also run to evaluate voxelwise WM variations between the study groups. Standard pre-processing, registration to the FMRIB58-FA standard-space image, and nonlinear transformation to all subjects' FA / RD images were implemented. [38] Voxelwise statistics on the skeletonized FA / RD maps were computed using FSL's *randomise* tool [39] with 5000 permutations, controlling for age and sex, and family-wise error-corrected (FWER) using threshold-free cluster enhancement (TFCE) with 2D optimization. [40] Given our study focused on the concordance of two WM methodologies, statistical comparisons were restricted to RD increases and FA reduction in ALS versus controls, since these are the predominant changes. The significance level was set to  $p_{\text{FWER}} < 0.01$  to extract only the most affected foci of pathology.

**Table 1**

The list of the 50 tracts evaluated and the number of successful segmentations in the ALS cohort ( $n = 132$ ).

Tract name	Correctly segmented	Tract name (continued)	Correctly segmented	Tract name (continued)	Correctly segmented
Arcuate fasciculus left	130	Inferior cerebellar peduncle left	119	Superior longitudinal fasciculus III left	119
Arcuate fasciculus right	126	Inferior cerebellar peduncle right	114	Superior longitudinal fasciculus III right	119
Anterior thalamic radiation left	116	Inferior occipito-frontal fasciculus left	120	Superior thalamic radiation left	113
Anterior thalamic radiation right	118	Inferior occipito-frontal fasciculus right	120	Superior thalamic radiation right	118
Corpus callosum: Rostrum	119	Inferior longitudinal fasciculus left	119	Uncinate fasciculus left	117
Corpus callosum: Genu	126	Inferior longitudinal fasciculus right	119	Uncinate fasciculus right	120
Corpus callosum: Rostral body	103	Middle cerebellar peduncle	121	Thalamo-premotor left	116
Corpus callosum: Anterior midbody	108	Optic radiation left	119	Thalamo-premotor right	109
Corpus callosum: Posterior midbody	123	Optic radiation right	119	Thalamo-parietal left	123
Corpus callosum: Isthmus	129	Parieto-occipital pontine left	119	Thalamo-parietal right	124
Corpus callosum: Splenium	122	Parieto-occipital pontine right	118	Thalamo-occipital left	119
Cingulum left	124	Superior cerebellar peduncle left	119	Thalamo-occipital right	119
Cingulum right	123	Superior cerebellar peduncle right	118	Striato-fronto-orbital left	120
Corticospinal tract left	114	Superior longitudinal fasciculus I left	123	Striato-fronto-orbital right	120
Corticospinal tract right	114	Superior longitudinal fasciculus I right	124	Striato-premotor left	119
Fronto-pontine tract left	117	Superior longitudinal fasciculus II left	122	Striato-premotor right	115
Fronto-pontine tract right	118	Superior longitudinal fasciculus II right	122		

3. Results

3.1. Demographics

The two-sample *t*-tests revealed no significant differences between (1) male controls (mean age = 60.96 years, standard deviation [SD] ±9.68) and male patients (mean age = 62.64 years, SD ±11.52; *t*(136) = -0.8689, *p* = 0.3864) and (2) female controls (mean age = 56.94 years, SD +/- 9.91) and female patients (mean age = 60.13 years, SD +/- 8.31; *t*(92) = -1.6815, *p* = 0.0960). This suggests that the reference groups (which were used for z-scoring) were adequately age-matched for both males and females. Similarly, the two-sample *t*-tests indicated appropriate age-matching of the male controls with the male blinded subjects (mean age = 60.52 years, SD ±13.88; *t*(96) = 0.1823, *p*

= 0.8558) as well as of the female controls with the female blinded subjects (mean age = 55.11 years, SD ±15.03; *t*(76) = 0.6481, *p* = 0.5189).

3.2. Z-score based approach

The list of the 50 white matter tracts, [18] and the number of patients where the segmentation was successful is presented for each tract in Table 1. Our approach permits the tract-wise evaluation of individual WM profiles and the affected tracts can either be presented visually or listed as a text file. In Fig. 1 we provide an example for illustration; areas of FA reductions (Fig. 1A) and regions of increased RD (Fig. 1B) are presented in a 72-year-old male patient in 3D. Our algorithm also provides a summary text file for individual subjects (Fig. 1C) listing the

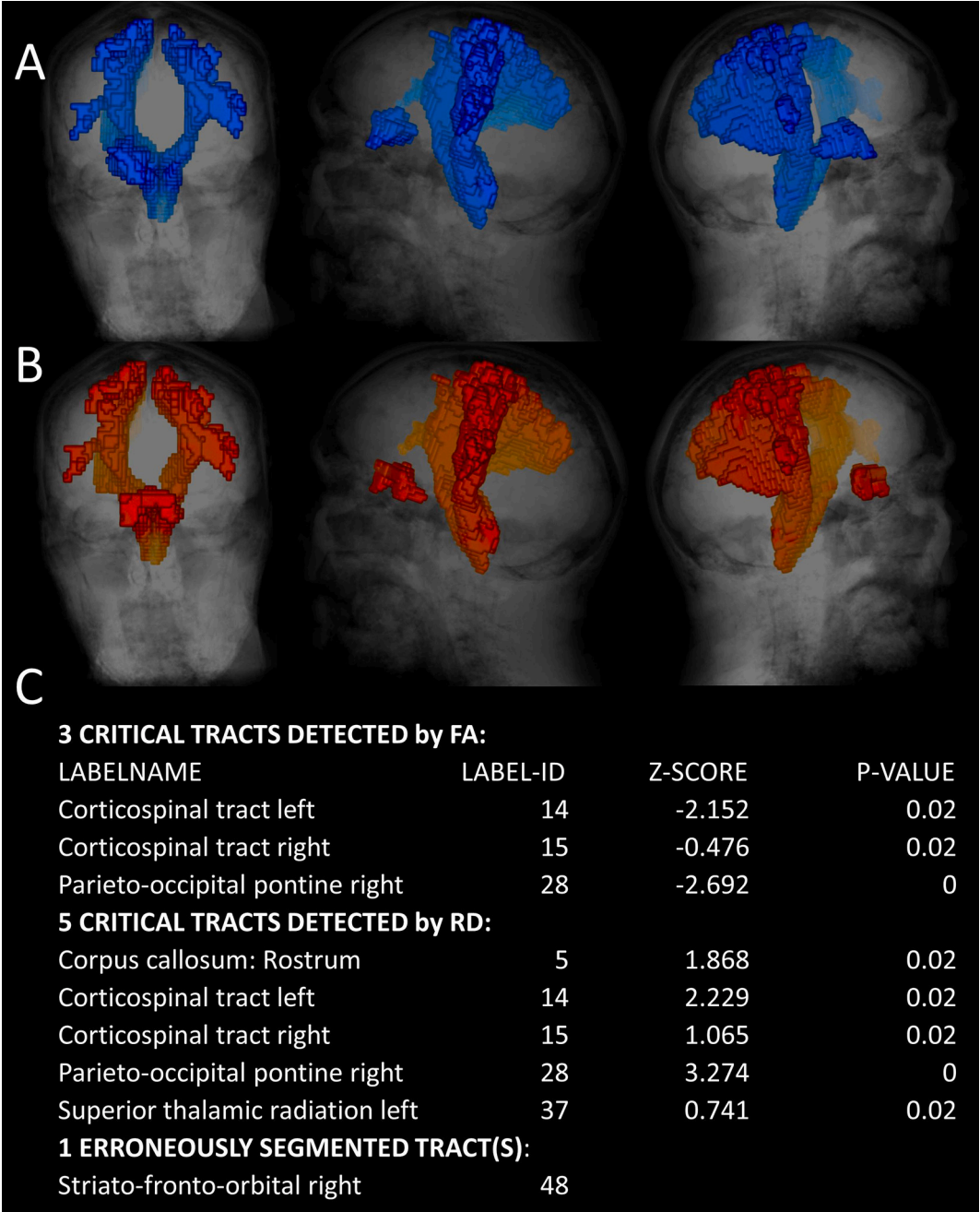


**Fig. 1.** White matter involvement in an individual ALS patient illustrating the z-score based data interpretation strategy with reference to demographically-matched controls. Outputs can be either presented visually or as text. Areas of FA reductions (A), regions of increased RD (B) are presented visually and affected tracts are listed as text (C).



affected tracts based on normative FA and RD, corresponding z-scores and p-values, and a list of tracts where WM segmentation failed, if applicable. In this patient, segmentation of the right striato-fronto-orbital tract failed. Both diffusivity metrics revealed left and right corticospinal tract degeneration. RD additionally detected corpus callosum and superior thalamic radiation involvement. The same output, visual and text, has been generated for each individual subject.

3.3. Group statistics

Permutation testing was used to highlight which tracts were affected across the entire ALS cohort using to the z-score-based approach. This analysis revealed a multitude of affected tracts, both based on FA alterations (Fig. 2A, Table 2) and RD changes (Fig. 2B, Table 3). Tables 2 and 3 rank the most affected tracts, revealing widespread white matter degeneration and suggesting that RD may be more sensitive in detecting integrity changes than FA.

3.4. Tract-based spatial statistics

Fig. 3 depicts group-level observations from the ‘standard approach’ using tract-based spatial statistics (TBSS). Both patterns of FA reductions (Fig. 3A) and RD increases (Fig. 3B) are widespread with the relative sparing of some posterior and cerebellar tracts. The anatomical patterns identified by TBSS are largely congruent with the group-level outputs of the z-score based strategy. Similar to the z-score based approach, RD detected slightly more affected tracts than FA.

3.5. Pilot-classification

The text outputs of 78 subjects with a blinded diagnosis were reviewed separately of the descriptive analyses presented above. These subjects were not part of the group-level statistics presented previously, z-scored or TBSS. In the pilot classification part of the study, 53 patients with ALS and 25 HC were included. Based on the individual text output of the blinded subjects, thirty-nine out of the 53 ALS patients were correctly identified as subjects with ALS (73.58%) and 19 of the 25 healthy individuals (76%) were also correctly identified based on their

Table 2

Tracts with significant fractional anisotropy (FA) reductions in the ALS group.

Tract name	P <sub>FWER</sub>
Arcuate fasciculus left	0.0171
Corpus callosum: Genu	0.0004
Corpus callosum: Isthmus	0.0164
Corpus callosum: Splenium	0.0038
Corticospinal tract right	<0.0001
Inferior occipito-frontal fasciculus left	0.0009
Middle cerebellar peduncle	0.0001
Optic radiation left	0.0033
Superior longitudinal fasciculus I left	0.0002
Superior longitudinal fasciculus III right	0.0008

white matter profiles.

4. Discussion

Our findings indicate that diffusion data from single subjects may be interpreted if a moderate sized control dataset is available.

In ALS, the visual inspection of white matter changes on FLAIR and T2 datasets offers limited insights. Qualitative cues, such as hyperintensities along the corticospinal tracts and thinning of the corpus callosum have been observed in ALS, but the specificity and sensitivity of these findings are relatively limited and may depend on pulse sequence settings and disease duration. [41,42] The visual inspection of diffusion tensor data offers no meaningful information with regards to pathological changes and is merely suitable for the assessment of gross imaging artifacts pertaining to movement, susceptibility-relation distortions, or eddy currents. The visual evaluation of T1- and T2-weighted data may suggest cortical grey matter atrophy qualitatively, but one cannot comment on white matter atrophy based on these pulse sequences. Quantitative group comparisons of patients with an established diagnosis and healthy controls have consistently captured corpus callosum degeneration and corticospinal tract changes in ALS irrespective of the underlying phenotype or genotype. [43–45] Unlike in PLS, [46] the clinical detection of the extent of pyramidal tract degeneration is confounded by co-existing lower motor neuron dysfunction.

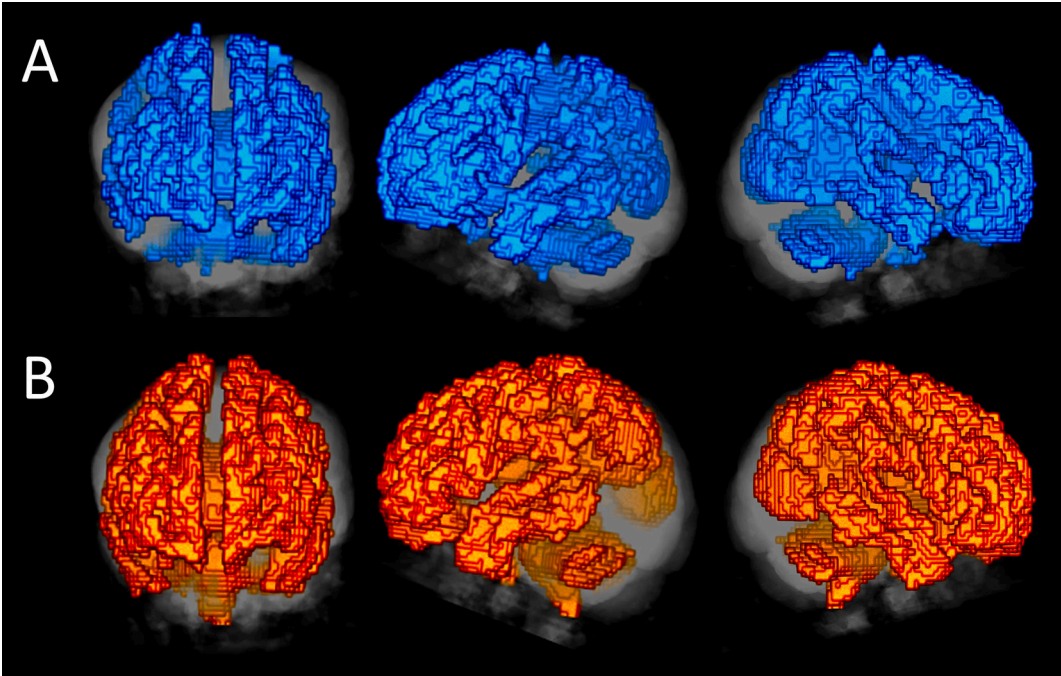


Fig. 2. Group-level findings derived from the z-scoring approach. Regions of fractional anisotropy reduction (A), and areas of increased radial diffusivity (B).

**Table 3**

Tracts with significant radial diffusivity (RD) increase in the ALS group.

Tract name	P <sub>FWER</sub>	Tract name	P <sub>FWER</sub>
Arcuate fasciculus left	0.0001	Parieto-occipital pontine left	<0.0001
Arcuate fasciculus right	0.0004	Parieto-occipital pontine right	0.0009
Corpus callosum: Rostrum	<0.0001	Superior cerebellar peduncle left	<0.0001
Corpus callosum: Genu	0.0010	Superior cerebellar peduncle right	<0.0001
Corpus callosum: Rostral body	0.0003	Superior longitudinal fasciculus I left	<0.0001
Corpus callosum: Anterior midbody	0.0016	Superior longitudinal fasciculus I right	<0.0001
Corpus callosum: Posterior midbody	0.0010	Superior longitudinal fasciculus II left	0.0003
Corpus callosum: Isthmus	0.0015	Superior longitudinal fasciculus III left	0.0002
Cingulum left	0.0013	Superior longitudinal fasciculus III right	0.0001
Corticospinal tract left	<0.0001	Superior thalamic radiation left	<0.0001
Corticospinal tract right	<0.0001	Superior thalamic radiation right	<0.0001
Fronto-pontine tract right	0.0030	Uncinate fasciculus left	<0.0001
Inferior cerebellar peduncle left	0.0035	Uncinate fasciculus right	<0.0001
Inferior cerebellar peduncle right	0.0001	Thalamo-parietal right	0.0131
Inferior occipito-frontal fasciculus right	<0.0001	Thalamo-occipital right	0.0107
Middle cerebellar peduncle	<0.0001	Striato-fronto-orbital right	0.0036
Optic radiation right	0.0030		

Corticospinal tract changes in ALS can be readily detected along the entire cerebral course of the pyramidal tracts in ALS from the corona radiata, through the posterior limb of the internal capsule to the brainstem. [47,48] A variety of white matter imaging methods have been implemented in ALS including spherical deconvolution, fixel-based approaches, neurite orientation dispersion and density imaging (NODDI), and diffusion tensor imaging as well as non-diffusion methods such as volumetry, morphometry and spectroscopy. [49–53] Diffusion data in ALS is most commonly interrogated by tract-based methods or tractography. [54] Despite the success and relative consistency of these studies, their drawback is that the statistical maps present shared white matter signatures and do not directly represent alterations in single subjects.

In this study we have detected the involvement of relevant white matter tracts in single subjects with reference to demographically matched controls without relying on other subjects from the same patient cohort. The mathematical model utilised is relatively simple and centres on z-scoring variables based on normative data. This concept is widely utilised in medicine for the evaluation of metrics in single subjects spanning from neuropsychological assessments, the interpretation of serum markers, appraisal of developmental scores and in a variety of biomarker applications. [55,56] We have successfully detected white matter changes in individual subjects, but our approach also permitted the contrasting of patients and controls at a group-level, which facilitates validation by conventional tract-based statistics. We have identified good concordance between the z-score-based approach and standard TBSS.

To model a potential clinical application, we have evaluated 78 subjects independently, where the diagnosis was blinded from the first author. This cohort included 53 subjects who were scanned within 3 months of their diagnosis and 25 healthy controls. By rating their white matter profile, 73.5% of the ALS subjects were correctly diagnosed on the basis of corpus callosum and corticospinal tract involvement. 76% of

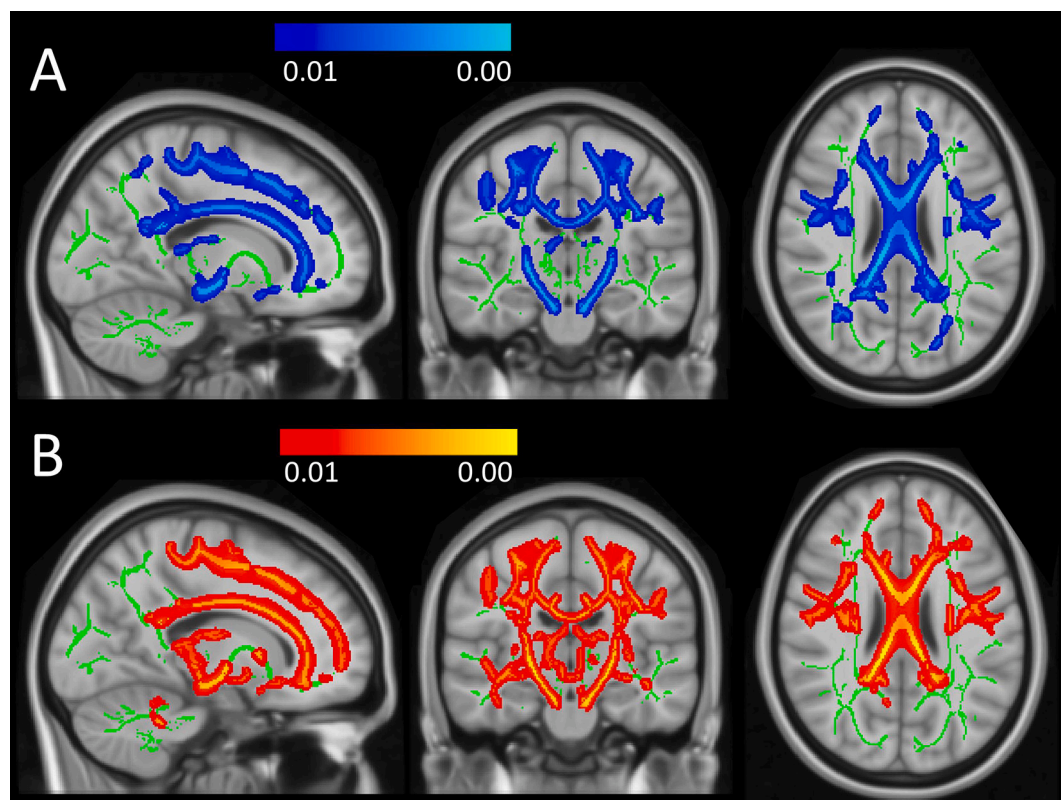


**Fig. 3.** Group comparisons using tract-based spatial statistics. Regions of decreased fractional anisotropy at  $p < 0.01$  (A) and areas of increased radial diffusivity at  $p < 0.01$  (B). Statistical outputs are corrected for age, sex, and family-wise error.

the healthy controls were correctly identified as healthy individuals on the basis of the absence of white matter abnormalities with respect to normative data. While this is merely a pilot study to evaluate single subjects' white matter microstructure in a simulated diagnostic scenario, it demonstrates the feasibility of this strategy. There are obvious considerations to improve the accuracy of this framework, chief of which is the expansion of normative data to larger cohorts covering all demographic sub-groups and boosting the overall numbers in each group. A more fine-grained categorisation of controls such as the inclusion age-ranges, and education bands would no doubt improve the performance of such schemes further. There is evidence that education impacts on white matter integrity especially in extra-motor regions [57] and using narrow age-range control subgroups would permit superior demographic matching. The combination of white matter measures with grey matter metrics is likely to improve the diagnostic classification of individual subjects further. [58] The testing of this white matter rating scheme in presymptomatic mutation carriers would lend further credence to the validity of this approach. [4,59] A natural expansion of this strategy is the inclusion of non-ALS neurodegenerative cohorts and disease mimics, which is beyond the scope of this present study. [60]

Another benefit of quantitative imaging in ALS is the precision staging of patients based on disease burden patterns. Clinical staging systems have proven useful for a variety of clinical applications spanning from accurate patient stratification to predictive modelling. [61] Diffusion imaging has shown promise to categorise patients *in vivo* according to pathological TDP-43 stages. [48,62] The automated listing of affected tracts based on quantitative measures would also permit the tracking of longitudinal changes in single patients. Longitudinal cohort studies often use mixed effect models and correct for the effects of healthy aging, [63] but group-level observations may be of limited interest in the management and tracking of individual patients. In multidisciplinary team (MDT) clinics, the focus is the follow-up of individual patients and the assessment of accruing disease burden with reference to earlier scans in the same patients. This is in line with the principles of 'precision medicine' and enables the assessment of progression rates, helps the timing of interventions, foreseeing management challenges and informs resource allocation. [64]

The detection of white matter changes outside the pyramidal system is consistent with the evolving literature of neuropsychological and extrapyramidal deficits in ALS. [65–68] Once regarded as a pure motor neuron disorder, ALS is now universally recognised as a condition with overlapping clinical, radiological and genetic features with frontotemporal dementia (FTD). The ascertainment of frontotemporal WM alterations may guide physicians and the MDT team to screen for incipient cognitive or behavioural deficits and tailor their management strategies accordingly. [69,70] Initially, ALS was primarily associated with deficits in executive dysfunction, but the gamut of possible manifestations also includes language deficits, deficits in social cognition, apathy as well as other cognitive domains. [10,71–74] In our study, we found evidence of left arcuate fasciculus, superior longitudinal fasciculus, inferior occipito-frontal fasciculus, middle cerebellar peduncle and optic radiation involvement based on FA and RD. The role of the left arcuate fasciculus (AF) is relatively well established in processing complex sequences of syntax and its involvement supports the large body of literature pertaining to language deficits in ALS. [75–77] Cerebellar peduncle involvement in ALS is relatively well recognised, [54,78–80], but its clinical manifestations remain to be clarified. [81–84] Our study highlights that the involvement of the long association fibres, such as the superior longitudinal fasciculus (SLF) is a relatively core feature of ALS and not unique to smaller subgroups.

One of the other advantages of a z-scored based approach is the opportunity to interpret radiological findings with respect to sex-matched cohorts. The physiological sexual dimorphism of neuroradiological metrics is widely recognised and sexual dimorphism is also an important factor in ALS. [85–87] Most ALS studies combine male and female patients and correct for sex as a covariate in the statistical

models. A z-score based approach allows the interpretation of an individual scan based on sex-matched controls alone. It is conceivable that other imaging metrics, such as network coherence measures, metabolite ratios, cord parameters, subcortical grey matter indices, quantitative susceptibility mapping (QSM) measures may also be interpreted in a similar fashion. [88–94] While the implementation of the z-scoring scheme requires computational resources compared to the visual review of MR images, it can be readily implemented on local radiology servers or on cloud-based platforms without introducing delays to reporting.

This study is merely a demonstration of how a single DTI data set may be interpreted in a low-incidence neurodegenerative condition. This is a proof-of-concept study of white matter interpretation and is not meant as a fully developed diagnostic framework. A number of limitations need to be acknowledged which need further optimisation for the concept to be transferable to clinical practice. First and foremost, a larger reference dataset is required, ideally also stratified for age and education. This method examines the integrity of tracts along their entire course and does not take segmental changes into consideration. The assessment of blinded data is not a validation of the approach, merely a pilot analysis, modelling clinical scenarios. A shortcoming of the labelling of blinded datasets is the binary categorised into 'ALS' or 'HC' instead of also considering a tertiary label of 'alternative diagnosis'. Real-life diagnostic dilemmas typically centre on the categorisation of an early-stage symptomatic patient as 'likely ALS' versus an alternative neurodegenerative condition (PLS, HSP, etc.) [95,96] Finally, the applicability of our approach may be limited in lower motor neuron-predominant MNDs such as SBMA, SMA, Polio, or PMA, where disease burden is primarily in the spinal anterior horns and not cerebral. [97–100] Notwithstanding these limitations, our study demonstrates the feasibility of interpreting single diffusion data sets.

## 5. Conclusions

Amyotrophic lateral sclerosis is not only associated with corpus callosum and corticospinal tract degeneration, but the cerebellar peduncles, arcuate fasciculus and long association fibres are also commonly involved. These changes can be readily detected in single patients and a list of affected fibre bundles can be generated if normative datasets have been previously compiled. The presented approach may also be successfully applied to patients in their peri-diagnostic phase. While the description of group-level signatures is of academic interest, future imaging studies should focus on the development and validation of methods to classify single datasets into diagnostic and prognostic groups.

## Funding

Professor Peter Bede and the Computational Neuroimaging Group are supported by the Health Research Board (HRB EIA-2017-019), the Spastic Paraplegia Foundation (SPF), the EU Joint Programme – Neurodegenerative Disease Research (JPND), the Andrew Lydon Scholarship, the Irish Institute of Clinical Neuroscience (IICN), and the Iris O'Brien Foundation. MT was supported by the German Multiple Sclerosis Society (Deutsche Multiple Sklerose Gesellschaft, DMSG).

## Research ethics approval

This study was approved by the Ethics (Medical Research) Committee—Beaumont Hospital, Dublin, Ireland.

## Contributorship

Conceptualisation of the study: MT, PB.

Drafting the manuscript: MT, AM, PB.

Neuroimaging analyses: MT, AM, JL, PB.

Revision of the manuscript for intellectual content: MT, AM, JL, OH,



PB.

## Declaration of Competing Interest

The authors have no competing interests to declare.

## Acknowledgments

We thank all participating patients and each healthy control for supporting this research study. Without their contribution, this study would not have been possible. We also express our gratitude to the caregivers and family members of patients with ALS for facilitating attendance at our neuroimaging centre. We also thank all patients who had expressed interest in the study but could not participate due to medical or logistical reasons.

## References

- [1] J. Wen, et al., Neurite density is reduced in the presymptomatic phase of C9orf72 disease, *J. Neurol. Neurosurg. Psychiatry* 90 (4) (2019) 387–394.
- [2] G. Querin, et al., Presymptomatic spinal cord pathology in C9orf72 mutation carriers: a longitudinal neuroimaging study, *Ann. Neurol.* 86 (2) (2019) 158–167.
- [3] A. Bertrand, et al., Early cognitive, structural, and microstructural changes in Presymptomatic C9orf72 carriers younger than 40 years, *JAMA Neurol.* 75 (2) (2018) 236–245.
- [4] R.H. Chipika, et al., The presymptomatic phase of amyotrophic lateral sclerosis: are we merely scratching the surface? *J. Neurol.* (2020) <https://doi.org/10.1007/s00415-020-10289-5>. Online ahead of print.
- [5] R.A. Menke, et al., Increased functional connectivity common to symptomatic amyotrophic lateral sclerosis and those at genetic risk, *J. Neurol. Neurosurg. Psychiatry* 87 (6) (2016) 580–588.
- [6] D.E. Lulé, et al., Deficits in verbal fluency in presymptomatic C9orf72 mutation gene carriers—a developmental disorder, *J. Neurol. Neurosurg. Psychiatry* 91 (2020) 1195–1200.
- [7] C. Schuster, et al., The segmental diffusivity profile of amyotrophic lateral sclerosis associated white matter degeneration, *Eur. J. Neurol.* 23 (8) (2016) 1361–1371.
- [8] T. Prell, J. Grosskreutz, The involvement of the cerebellum in amyotrophic lateral sclerosis, *Amyotroph. Lateral Scler. Frontotemporal. Degener.* 14 (7–8) (2013) 507–515.
- [9] P. Bede, et al., Patterns of cerebral and cerebellar white matter degeneration in ALS, *J. Neurol. Neurosurg. Psychiatry* 86 (4) (2015) 468–470.
- [10] F. Trojsi, et al., Frontotemporal degeneration in amyotrophic lateral sclerosis (ALS): a longitudinal MRI one-year study, *CNS Spectr.* (2020) 1–10.
- [11] F. Christidi, et al., Hippocampal pathology in amyotrophic lateral sclerosis: selective vulnerability of subfields and their associated projections, *Neurobiol. Aging* 84 (2019) 178–188.
- [12] F. Christidi, et al., Clinical and radiological markers of extra-motor deficits in amyotrophic lateral sclerosis, *Front. Neurol.* 9 (2018) 1005.
- [13] T. Omer, et al., Neuroimaging patterns along the ALS-FTD spectrum: a multiparametric imaging study, *Amyotroph. Lateral Scler. Frontotemporal. Degener.* 18 (7–8) (2017) 611–623.
- [14] H.J. Westeneng, et al., Widespread structural brain involvement in ALS is not limited to the C9orf72 repeat expansion, *J. Neurol. Neurosurg. Psychiatry* 87 (12) (2016) 1354–1360.
- [15] E. Verstraete, et al., Mind the gap: the mismatch between clinical and imaging metrics in ALS, *Amyotroph. Lateral Scler. Frontotemporal. Degener.* 16 (7–8) (2015) 524–529.
- [16] R.A. Menke, et al., Widespread grey matter pathology dominates the longitudinal cerebral MRI and clinical landscape of amyotrophic lateral sclerosis, *Brain* 137 (Pt 9) (2014) 2546–2555.
- [17] P. Bede, O. Hardiman, Longitudinal structural changes in ALS: a three time-point imaging study of white and gray matter degeneration, *Amyotroph. Lateral Scler. Frontotemporal. Degener.* 19 (3–4) (2018) 232–241.
- [18] R.C. Welsh, L.M. Jelsone-Swain, B.R. Foerster, The utility of independent component analysis and machine learning in the identification of the amyotrophic lateral sclerosis diseased brain, *Front. Hum. Neurosci.* 7 (2013) 251.
- [19] C. Schuster, O. Hardiman, P. Bede, Development of an automated MRI-based diagnostic protocol for amyotrophic lateral sclerosis using disease-specific pathognomonic features: a quantitative disease-state classification study, *PLoS One* 11 (12) (2016), e0167331.
- [20] C. Schuster, O. Hardiman, P. Bede, Survival prediction in amyotrophic lateral sclerosis based on MRI measures and clinical characteristics, *BMC Neurol.* 17 (1) (2017) 73.
- [21] P. Bede, et al., Virtual brain biopsies in amyotrophic lateral sclerosis: diagnostic classification based on in vivo pathological patterns, *Neuroimage Clin.* 15 (2017) 653–658.
- [22] G. Querin, et al., Multimodal spinal cord MRI offers accurate diagnostic classification in ALS, *J. Neurol. Neurosurg. Psychiatry* 89 (11) (2018) 1220–1221.
- [23] P. Bede, From qualitative radiological cues to machine learning: MRI-based diagnosis in neurodegeneration, *Future Neurol.* 12 (1) (2017) 5–8.
- [24] V. Grollemund, et al., Machine learning in amyotrophic lateral sclerosis: achievements, pitfalls, and future directions, *Front. Neurosci.* 13 (2019) 135.
- [25] J.D. Tournier, et al., MRtrix3: a fast, flexible and open software framework for medical image processing and visualisation, *NeuroImage* 202 (2019) 116137.
- [26] J. Veraart, E. Fieremans, D.S. Novikov, Diffusion MRI noise mapping using random matrix theory, *Magn. Reson. Med.* 76 (5) (2016) 1582–1593.
- [27] J. Veraart, et al., Denoising of diffusion MRI using random matrix theory, *NeuroImage* 142 (2016) 394–406.
- [28] E. Kellner, et al., Gibbs-ringing artifact removal based on local subvoxel-shifts, *Magn. Reson. Med.* 76 (5) (2016) 1574–1581.
- [29] S.M. Smith, et al., Advances in functional and structural MR image analysis and implementation as FSL, *NeuroImage* 23 (Suppl. 1) (2004) S208–S219.
- [30] N.J. Tustison, et al., N4ITK: improved N3 bias correction, *IEEE Trans. Med. Imaging* 29 (6) (2010) 1310–1320.
- [31] P.J. Basser, J. Mattiello, D. LeBihan, MR diffusion tensor spectroscopy and imaging, *Biophys. J.* 66 (1) (1994) 259–267.
- [32] M. Jenkinson, et al., FSL, *NeuroImage* 62 (2) (2012) 782–790.
- [33] M.W. Woolrich, et al., Bayesian analysis of neuroimaging data in FSL, *NeuroImage* 45 (1) (2009) S173–S186.
- [34] T. Dhollander, D. Raffelt, A. Connelly, Unsupervised 3-tissue response function estimation from single-shell or multi-shell diffusion MR data without a co-registered T1 image, in: Conference: ISMRM Workshop on Breaking the Barriers of Diffusion MRI, 2016 (Lisbon, Portugal).
- [35] D. Raffelt, et al., Bias field correction and intensity normalisation for quantitative analysis of apparent fibre density, *Proc. ISMRM* 26 (2017) 3541.
- [36] B. Jeurissen, et al., Investigating the prevalence of complex fiber configurations in white matter tissue with diffusion magnetic resonance imaging, *Hum. Brain Mapp.* 34 (11) (2013) 2747–2766.
- [37] J. Wasserthal, P. Neher, K.H. Maier-Hein, TractSeg - fast and accurate white matter tract segmentation, *NeuroImage* 183 (June) (2018) 239–253.
- [38] M. Bach, et al., Methodological considerations on tract-based spatial statistics (TBSS), *NeuroImage* 100 (2014) 358–369.
- [39] A.M. Winkler, et al., Permutation inference for the general linear model, *NeuroImage* 92 (2014) 381–397.
- [40] S.M. Smith, T.E. Nichols, Threshold-free cluster enhancement: addressing problems of smoothing, threshold dependence and localisation in cluster inference, *NeuroImage* 44 (1) (2009) 83–98.
- [41] P. Bede, R.H. Chipika, Commissural fiber degeneration in motor neuron diseases, *Amyotroph. Lateral Scler. Frontotemporal. Degener.* (2020) 1–3.
- [42] V. Rajagopalan, E.P. Piore, Unbiased MRI analyses identify micro-pathologic differences between upper motor neuron-predominant ALS phenotypes, *Front. Neurosci.* 13 (2019) 704.
- [43] N. Filippini, et al., Corpus callosum involvement is a consistent feature of amyotrophic lateral sclerosis, *Neurology* 75 (18) (2010) 1645–1652.
- [44] H.P. Müller, et al., Segmental involvement of the corpus callosum in C9orf72-associated ALS: a tract of interest-based DTI study, *Ther. Adv. Chronic. Dis.* 12 (2021) (p. 204062232111002969).
- [45] H.P. Müller, et al., A large-scale multicentre cerebral diffusion tensor imaging study in amyotrophic lateral sclerosis, *J. Neurol. Neurosurg. Psychiatry* 87 (6) (2016) 570–579.
- [46] E. Finegan, et al., The clinical and radiological profile of primary lateral sclerosis: a population-based study, *J. Neurol.* 266 (11) (2019) 2718–2733.
- [47] R.A. Menke, et al., Fractional anisotropy in the posterior limb of the internal capsule and prognosis in amyotrophic lateral sclerosis, *Arch. Neurol.* 69 (11) (2012) 1493–1499.
- [48] J. Kassubek, et al., Diffusion tensor imaging analysis of sequential spreading of disease in amyotrophic lateral sclerosis confirms patterns of TDP-43 pathology, *Brain* 137 (Pt 6) (2014) 1733–1740.
- [49] V. Govind, et al., Comprehensive evaluation of corticospinal tract metabolites in amyotrophic lateral sclerosis using whole-brain 1H MR spectroscopy, *PLoS One* 7 (4) (2012), e35607.
- [50] A.W. Barritt, et al., Emerging magnetic resonance imaging techniques and analysis methods in amyotrophic lateral sclerosis, *Front. Neurol.* 9 (2018) 1065.
- [51] R.J. Broad, et al., Neurite orientation and dispersion density imaging (NODDI) detects cortical and corticospinal tract degeneration in ALS, *J. Neurol. Neurosurg. Psychiatry* 90 (4) (2019) 404–411.
- [52] D.A. Raffelt, et al., Connectivity-based fixel enhancement: whole-brain statistical analysis of diffusion MRI measures in the presence of crossing fibres, *Neuroimage* 117 (2015) 40–55.
- [53] P. Stämpfli, et al., Investigation of neurodegenerative processes in amyotrophic lateral sclerosis using white matter fiber density, *Clin. Neuroradiol.* 29 (3) (2019) 493–503.
- [54] P. Bede, et al., Genotype-associated cerebellar profiles in ALS: focal cerebellar pathology and cerebro-cerebellar connectivity alterations, *J. Neurol. Neurosurg. Psychiatry* (2021), <https://doi.org/10.1136/jnnp-2021-326854>. Online ahead of print, PMID: 34168085.
- [55] H. Blasco, et al., A pharmaco-metabolomics approach in a clinical trial of ALS: identification of predictive markers of progression, *PLoS One* 13 (6) (2018), e0198116.
- [56] D. Devos, et al., A ferroptosis-based panel of prognostic biomarkers for Amyotrophic Lateral Sclerosis, *Sci. Rep.* 9 (1) (2019) 2918.
- [57] J. Bathelt, et al., Whole-brain white matter organization, intelligence, and educational attainment, *Trends Neurosci. Educ.* 15 (2019) 38–47.
- [58] M. Tahedi, et al., Cortical progression patterns in individual ALS patients across multiple timepoints: a mosaic-based approach for clinical use, *J. Neurol.* 268 (2021) 1913–1926.



- [59] C. Schuster, et al., Presymptomatic and longitudinal neuroimaging in neurodegeneration—from snapshots to motion picture: a systematic review, *J. Neurol. Neurosurg. Psychiatry* 86 (10) (2015) 1089–1096.
- [60] Medical mimics of neurodegenerative diseases, in: L. Rowland, et al. O. Hardiman, et al. (Eds.), *Neurodegenerative Disorders*, Springer, Cham: London, 2016, pp. 199–212.
- [61] F. Trojsi, et al., High angular resolution diffusion imaging abnormalities in the early stages of amyotrophic lateral sclerosis, *J. Neurol. Sci.* 380 (2017) 215–222.
- [62] H.P. Müller, et al., In vivo histopathological staging in C9orf72-associated ALS: a tract of interest DTI study, *Neuroimage Clin.* 27 (2020) 102298.
- [63] R.H. Chipika, et al., Tracking a fast-moving disease: longitudinal markers, monitoring, and clinical trial endpoints in ALS, *Front. Neurol.* 10 (2019) 229.
- [64] D. Oliver, et al., Palliative care and end of life care, in: O. Hardiman, et al. (Eds.), *Neurodegenerative Disorders*, Springer, Cham: London, 2016, pp. 305–319.
- [65] F. Christidi, et al., The clinical and radiological spectrum of hippocampal pathology in amyotrophic lateral sclerosis, *Front. Neurol.* 9 (2018) 523.
- [66] M. Abidi, et al., Neural correlates of motor imagery of gait in amyotrophic lateral sclerosis, *J. Magn. Reson. Imaging* 53 (2020) 223–233.
- [67] M. Feron, et al., Extrapyramidal deficits in ALS: a combined biomechanical and neuroimaging study, *J. Neurol.* 265 (9) (2018) 2125–2136.
- [68] M. Abidi, et al., Adaptive functional reorganization in amyotrophic lateral sclerosis: coexisting degenerative and compensatory changes, *Eur. J. Neurol.* 27 (1) (2020) 121–128.
- [69] T. Burke, et al., Visual encoding, consolidation, and retrieval in amyotrophic lateral sclerosis: executive function as a mediator, and predictor of performance, *Amyotroph. Lateral Scler. Frontotemporal. Degener.* 18 (3–4) (2017) 193–201.
- [70] T. Burke, et al., A cross-sectional population-based investigation into behavioral change in amyotrophic lateral sclerosis: subphenotypes, staging, cognitive predictors, and survival, *Ann. Clin. Transl. Neurol.* 4 (5) (2017) 305–317.
- [71] D. Lule, et al., Emotional adjustment in amyotrophic lateral sclerosis (ALS), *J. Neurol.* 259 (2) (2012) 334–341.
- [72] T. Burke, et al., Discordant performance on the 'Reading the Mind in the Eyes' Test, based on disease onset in amyotrophic lateral sclerosis, *Amyotroph. Lateral Scler. Frontotemporal. Degener.* (2016) 1–6.
- [73] T. Burke, et al., Measurement of social cognition in amyotrophic lateral sclerosis: a population based study, *PLoS One* 11 (8) (2016), e0160850.
- [74] M. Pinto-Grau, O. Hardiman, N. Pender, The study of language in the amyotrophic lateral sclerosis - frontotemporal spectrum disorder: a systematic review of findings and new perspectives, *Neuropsychol. Rev.* 28 (2) (2018) 251–268.
- [75] T.H. Bak, J.R. Hodges, Motor neurone disease, dementia and aphasia: coincidence, co-occurrence or continuum? *J. Neurol.* 248 (4) (2001) 260–270.
- [76] T.H. Bak, et al., Selective impairment of verb processing associated with pathological changes in Brodmann areas 44 and 45 in the motor neurone disease-dementia-aphasia syndrome, *Brain* 124 (2001) 103–120.
- [77] M. Grossman, et al., Impaired action knowledge in amyotrophic lateral sclerosis, *Neurology* 71 (18) (2008) 1396–1401.
- [78] J. Prudlo, et al., White matter pathology in ALS and lower motor neuron ALS variants: a diffusion tensor imaging study using tract-based spatial statistics, *J. Neurol.* 259 (9) (2012) 1848–1859.
- [79] S. Tu, et al., Cerebellar tract alterations in PLS and ALS, *Amyotroph. Lateral Scler. Frontotemporal. Degener.* 20 (3–4) (2019) 281–284.
- [80] M.C. McKenna, et al., Infratentorial pathology in frontotemporal dementia: cerebellar grey and white matter alterations in FTD phenotypes, *J. Neurol.* (2021), <https://doi.org/10.1007/s00415-021-10575-w>. Online ahead of print, PMID: 33983551.
- [81] E. Finegan, et al., Pathological crying and laughing in motor neuron disease: pathobiology, screening, intervention, *Front. Neurol.* 10 (2019) 260.
- [82] P. Bede, E. Finegan, Revisiting the pathoanatomy of pseudobulbar affect: mechanisms beyond corticobulbar dysfunction, *Amyotroph. Lateral Scler. Frontotemporal. Degener.* 19 (1–2) (2018) 4–6.
- [83] F. Christidi, et al., Investigating the neuroanatomical substrate of pathological laughing and crying in amyotrophic lateral sclerosis with multimodal neuroimaging techniques, *Amyotroph. Lateral Scler. Frontotemporal. Degener.* 19 (1–2) (2018) 12–20.
- [84] M.K. Floeter, et al., Impaired corticopontocerebellar tracts underlie pseudobulbar affect in motor neuron disorders, *Neurology* 83 (7) (2014) 620–627.
- [85] E. Luders, A.W. Toga, P.M. Thompson, Why size matters: differences in brain volume account for apparent sex differences in callosal anatomy: the sexual dimorphism of the corpus callosum, *Neuroimage* 84c (2013) 820–824.
- [86] K. Menzler, et al., Men and women are different: diffusion tensor imaging reveals sexual dimorphism in the microstructure of the thalamus, corpus callosum and cingulum, *Neuroimage* 54 (4) (2011) 2557–2562.
- [87] P. Bede, et al., Sexual dimorphism in ALS: exploring gender-specific neuroimaging signatures, *Amyotroph. Lateral Scler. Frontotemporal. Degener.* 15 (3–4) (2014) 235–243.
- [88] G. Conte, et al., Amyotrophic lateral sclerosis phenotypes significantly differ in terms of magnetic susceptibility properties of the precentral cortex, *Eur. Radiol.* 31 (7) (2021) 5272–5280.
- [89] B. Nasserleslami, et al., Characteristic increases in EEG connectivity correlate with changes of structural MRI in amyotrophic lateral sclerosis, *Cereb. Cortex* 29 (1) (2019) 27–41.
- [90] J.M. Meier, et al., Connectome-based propagation model in amyotrophic lateral sclerosis, *Ann. Neurol.* 87 (5) (2020) 725–738.
- [91] S. Dukic, et al., Patterned functional network disruption in amyotrophic lateral sclerosis, *Hum. Brain Mapp.* 40 (16) (2019) 4827–4842.
- [92] E. Finegan, et al., Widespread subcortical grey matter degeneration in primary lateral sclerosis: a multimodal imaging study with genetic profiling, *Neuroimage Clin.* 24 (2019) 102089.
- [93] M.M. El Mendili, et al., Spinal cord imaging in amyotrophic lateral sclerosis: historical concepts-novel techniques, *Front. Neurol.* 10 (2019) 350.
- [94] G. Querin, et al., The spinal and cerebral profile of adult spinal-muscular atrophy: a multimodal imaging study, *Neuroimage Clin.* 21 (2019) 101618.
- [95] E. Finegan, et al., Evolving diagnostic criteria in primary lateral sclerosis: the clinical and radiological basis of “probable PLS”, *J. Neurol. Sci.* 417 (2020) 117052.
- [96] E. Finegan, et al., Primary lateral sclerosis: a distinct entity or part of the ALS spectrum? *Amyotroph. Lateral Scler. Frontotemporal. Degener.* 20 (3–4) (2019) 133–145.
- [97] M.V. Leboutoux, et al., Revisiting the spectrum of lower motor neuron diseases with snake eyes appearance on magnetic resonance imaging, *Eur. J. Neurol.* 21 (9) (2014) 1233–1241.
- [98] P.F. Pradat, et al., The French national protocol for Kennedy's disease (SBMA): consensus diagnostic and management recommendations, *Orphanet. J. Rare Dis.* 15 (1) (2020) 90.
- [99] S. Li Hi Shing, et al., Increased cerebral integrity metrics in poliomyelitis survivors: putative adaptation to longstanding lower motor neuron degeneration, *J. Neurol. Sci.* (2021) 117361.
- [100] S. Li Hi Shing, et al., Post-polio syndrome: more than just a lower motor neuron disease, *Front. Neurol.* 10 (2019) 773.